Characteristics Modeling of GaN Class-AB Dual-Band PA Under Different Temperature and Humidity Conditions

SHAOHUA ZHOU[ID], (Student Member, IEEE), AND ABHISHEK KUMAR JHA[ID], (Member, IEEE)
[1]School of Microelectronics, Tianjin University, Tianjin 300072, China
[2]Department of Electrical Engineering, Indian Institute of Technology Tirupati, Chittoor, Andhra Pradesh 517619, India

Corresponding author: Shaohua Zhou (zhoushaohua@tju.edu.cn)

ABSTRACT As the technology scales down, besides the CAD tools and design guidelines, understanding circuit performance degradation as a consequence of transistor degradation becomes essential for designers. Due to several adverse environmental conditions, the study of performance degradation in the power amplifier (PA) is very demanding research. In this paper, an RF PA is experimentally studied to observe various characteristic degradations in a broad range of operating temperature and humidity conditions. Based on a few key measurement points, a measurement-based modeling method is proposed to help designers make intelligent decisions to minimize the performance degradation effects. This method uses four two-dimensional interpolation models, and the results show that the prediction results of the four planar interpolation models are in good agreement with the measurement results. The results presented in this article help select design models for the RF power amplifier that can analyze the performance degradation of the transistor parameters in advance. Cubic and spline interpolation has the highest model accuracy among the four two-dimensional models, while the nearest interpolation offers the shortest training time.

INDEX TERMS Two-dimensional interpolation, power amplifier (PA), characteristics modeling, temperature, humidity.

I. INTRODUCTION

Power amplifiers (PAs) are commonly used in a variety of applications such as radar applications [1]–[6], imaging systems [7]–[9], wireless/mobile communications [10]–[13], satellite communications [14]–[17], positioning systems [18]–[21], etc. Some of these application systems have to be used in outdoor environments, for instance, the base stations of mobile communications [22]–[24], weather radar stations, etc., even under hazardous/extreme environments as well as fluctuating temperature and humidity [25]. It was reported that nearly 31% of system failures in the US coastal bases were caused by high temperature and humidity [26]. One of the major reasons for the electronic system failures is that the devices and the critical circuit elements cannot sustain extreme environmental conditions.

PAs are one of the critical circuit elements in any radio system to drive antennas, where antennas are used for transmission and receiving a signal through free space (usually air) [27]–[30]. Although it is well known that the behaviors of any PAs are strongly dependent on the temperature and humidity, the fluctuation in environmental conditions, primarily temperature [31]–[33], and humidity, causes the performance degradations of the PA [34]–[38].

In general, it is expected that a PA used in an RF system should maintain the specifications throughout its lifetime as initially designed and would not change no matter how the environmental conditions will vary. However, due to the lack of a comprehensive temperature and humidity dependent device model, their analysis and dependency in PA are confined to a limited temperature and humidity range [34]. When the ambient temperature and humidity exceed the simulated temperature and humidity range, the actual performance of the PA becomes far from the expected design performance [34]. Suppose a PA used in a system does not perform as designed/expected under certain environmental situations. In that case, the system's performances will be corrupted, even if the system is likely to fail [35], [36]. Therefore, it is desirable to get the PA's performance degradations concerning the temperature and humidity changes in advance.

The associate editor coordinating the review of this manuscript and approving it for publication was Giambattista Gruosso[ID].

Recently, an experimental analysis of aging due to the hot carrier injection (HCI) and bias temperature instability (BTI) effects in the 65-nm CMOS technology-based PA is presented in [39] that shows how aging produces important degradation carrier mobility and threshold voltage.

It is mainly due to the above reasons; the PA's performance degradation for the changes in temperature and humidity conditions is a hot topic of research [40]–[48]. However, most of the published papers are focused on the PA's performances degradations limited to the individual characteristic temperature and humidity, for instance, 85°/85%RH [40], 121°/100%RH [40], 0° [41], 25° [42], 50° [49], 80° [50], 100° [43], 130°/60%RH [44], 130°/40%RH [44]. Measurement of a PA's temperature and humidity dependence at specific temperature/humidity points does not provide enough information to model the relationships of the PA's performance degradations in actual environmental conditions [34]. The most direct method considers each temperature and humidity point to obtain the temperature and humidity characteristics in the whole temperature and humidity range. However, measuring all the temperature and humidity points is nearly impossible due to the limitation of measurement time, cost, and instruments.

This paper proposes a measurement-based modeling method to get a PA's temperature and humidity characteristics in the whole temperature and humidity range. The proposed technique provides a PA's complete environmental temperature and humidity characteristics by measuring a few critical temperatures and humidity points. This method uses planar interpolation to establish a nonlinear model, which can accurately predict the temperature and humidity characteristics of the PA in the entire range of temperature and humidity. Four types of planar interpolation methods are used to model PA's performance. They are based on two major environmental factors: two-dimensional linear interpolation, two-dimensional nearest interpolation, two-dimensional spline interpolation, and two-dimensional cubic interpolation. It is found that the measurement results are in good agreement with the predicted results using the proposed model.

This paper is organized as follows. First, the designed PA and the experimental setup are explained in Section II. Then, the modeling and result discussions are presented in Section III. Finally, conclusions are drawn in Section IV.

II. DESIGNED PA AND EXPERIMENTAL SETUP

A GaN class-AB dual-band power amplifier operating at 1.76 GHz/2.14 GHz is used for our experiment, as shown in Figure 1. The amplifier consisting of GaN HEMT (Cree's CGH40010F) has been fabricated on a Rogers 4350B substrate of thickness 30 mils with dielectric permittivity of 3.48. The total size of the board, including the heat sink, is 61.6 cm^2

The environmental test chamber (SC^3 1000 MHG from Vötsch Industrietechnik) has been used for environmental experiments and is shown in Figure 2. The dual-band power amplifier was tested under a combined temperature and
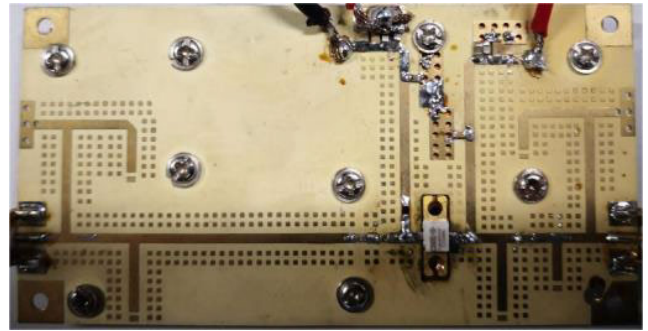

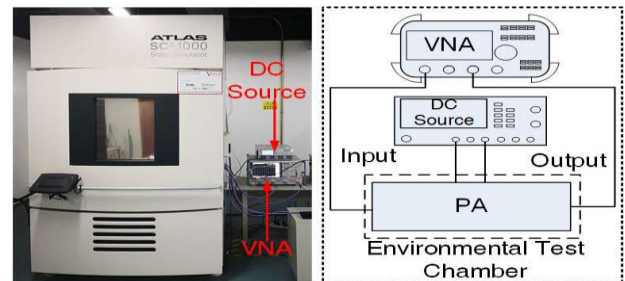**FIGURE 1.** The photograph of the GaN Class-AB dual-band PA.

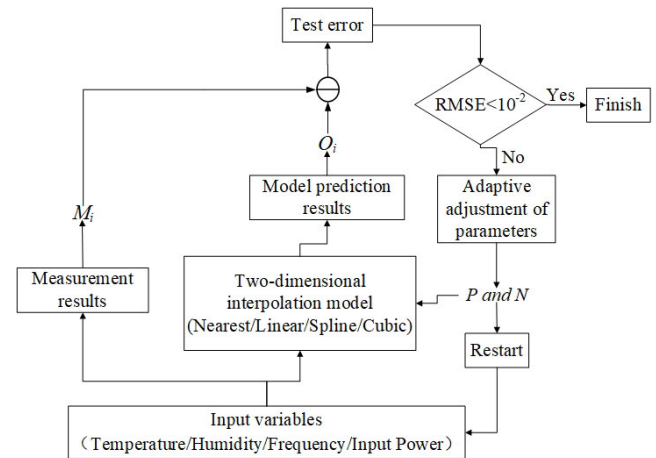**FIGURE 2.** The measurement environment and measurement setup.

FIGURE 3. The proposed measurement-based modeling process.

humidity condition where the humidity varies from 10%RH to 90%RH and the temperature varies from 10° to 90°.

The DC power supply HMP4040 of R&S provides a stable DC offset to the dual-band power amplifier during the environmental experiments. The measurement results are recorded using R&S Vector Network Analyzer (VNA) ZVA67.

III. MODELING AND RESULT DISCUSSIONS
A. MODELING
1) PROPOSED MEASUREMENT-BASED MODELING PROCESS
Two-dimensional interpolation is a standard and mature mathematical modeling method, which is also suitable for
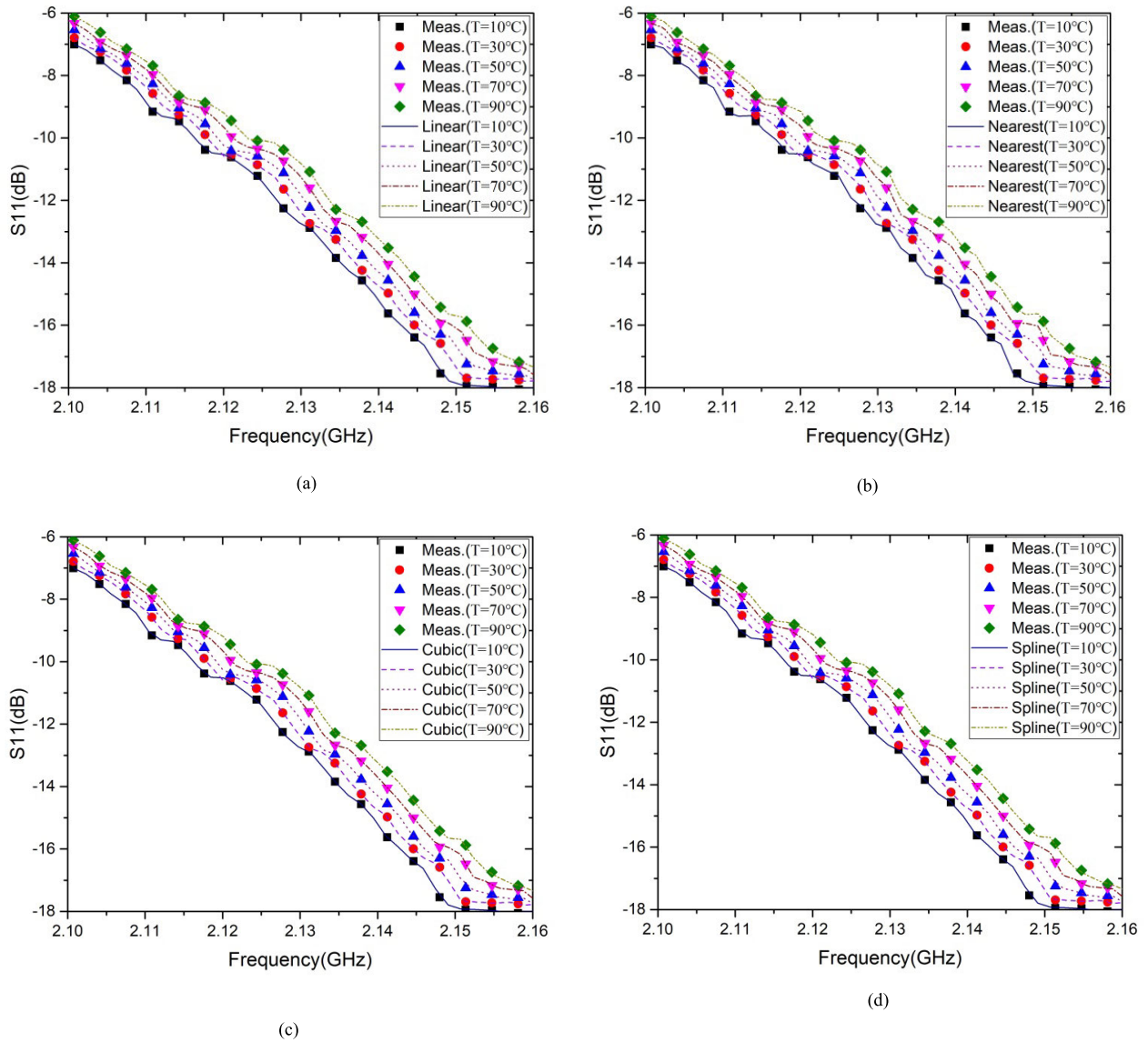
FIGURE 4. The modeling result of S_1 under different temperature: (a) two-dimensional linear interpolation; (b) two-dimensional nearest interpolation; (c) two-dimensional cubic interpolation; (d) two-dimensional spline interpolation.

nonlinear modeling problems and convenient to use at the system level. There is a strong nonlinear relationship between the temperature/humidity and the PA's performance and the relationship between the input and output [34], [51]. Therefore, to get the temperature and humidity characteristics of a PA in the whole temperature and humidity range, four different two-dimensional interpolation methods are used to model and predict the temperature and humidity characteristics of the PA.

The process of using two-dimensional interpolation to model and predict the performance of the PA in the broad range of temperature and humidity profiles is explained using the flow chart and shown in Figure 3.

As shown in Figure 3, the modeling process is quite generalized such that the input of the proposed model can be arbitrarily chosen. The input parameters in the above flow chart can be input power, frequency, voltage, and environmental conditions subject to the PA. This article mainly studies the temperature and humidity characteristics of the PA, so the input variables of the model in this article are input power, frequency, temperature, and humidity. The output of the proposed model includes output power, S-parameters, phase, impedance, power added efficiency (PAE), etc. For n arbitrary distinct samples (X_i, M_i), X_i is the input variable, and M_i is the measurement result. For each given example, the model will output a predicted value (O_i) accordingly. When the root mean square error (RMSE) between the model's expected value and the measured value is less than the required error accuracy requirement, the model is considered to have been trained. When the value of RMSE is greater than the error necessary accuracy, the model needs to be retrained. The sampling start position (P) and sampling
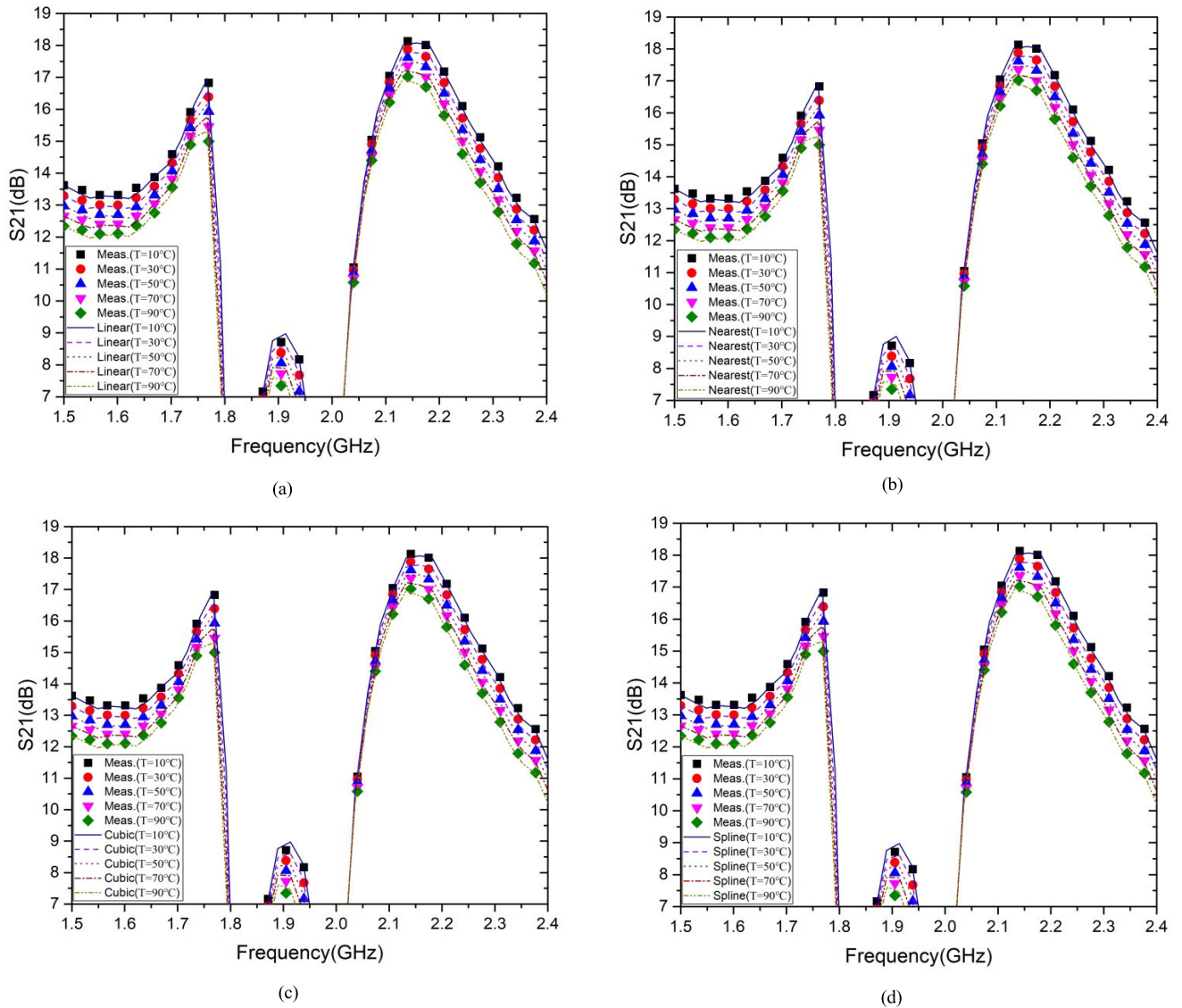
FIGURE 5. The modeling result of S$_{21}$ under different temperature: (a) two-dimensional linear interpolation; (b) two-dimensional nearest interpolation; (c) two-dimensional cubic interpolation; (d) two-dimensional spline interpolation.

interval (N) of the two-dimensional interpolation model can be adjusted to meet the required requirements during the retraining process.

2) TEST ERROR

After the model is trained, the measurement data is used to verify the accuracy of the trained model by calculating the RMSE of the difference between M_i and O_i as follows:

$$RMSE = \sqrt{\frac{1}{n}\sum_{i=1}^{n}(M_i - O_i)^2} \quad (1)$$

Only when the RMSE value is less than a threshold value, e.g., 10^{-2}, the trained model can be considered to meet the requirements. Otherwise, the model needs to be retrained until the RMSE value is less than the given value.

B. RESULT DISCUSSIONS

To comprehensively understand the relationships of the PA's performance degradations for the temperature and humidity changes in advance, four standard mathematical modeling methods, i.e., two-dimensional linear interpolation, two-dimensional nearest interpolation, two-dimensional spline interpolation, and two-dimensional cubic interpolation, have been introduced into the characteristics modeling of RF power amplifiers under different temperature and humidity conditions.

1) MODELING RESULT OF S$_{11}$ UNDER DIFFERENT TEMPERATURE

The four kinds of modeling results are estimated using the measured results of PA in the frequency range of 2.10 GHz − 2.16 GHz for various temperatures. The measured
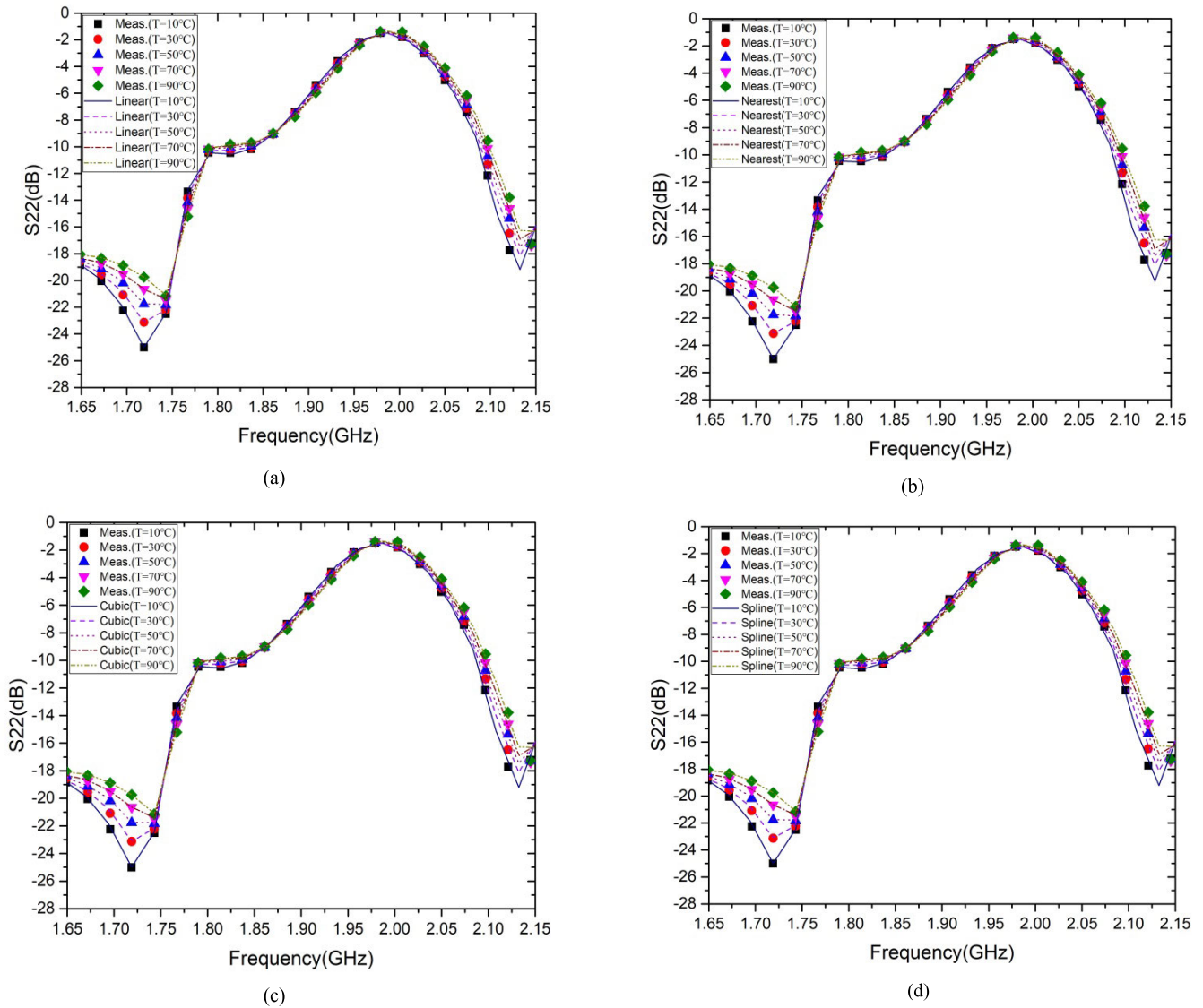
FIGURE 6. The modeling result of S$_{22}$ under different temperature: (a) two-dimensional linear interpolation; (b) two-dimensional nearest interpolation; (c) two-dimensional cubic interpolation; (d) two-dimensional spline interpolation.

reflection coefficients data and the modeled data are plotted together for each case and given in Figure 4. It is observed that the S$_{11}$ increases with increasing temperature. The main reason for this change is that the impedance of the transistor changes with the temperature, while the matching circuit has been processed and does not change with the temperature. Therefore, S$_{11}$ increases with the increase of temperature.

2) MODELING RESULT OF S$_{21}$ UNDER DIFFERENT TEMPERATURE

Similar to Figure 4, the modeling results of S$_{21}$ derived using the measured results of PA subjected to various temperatures are shown in Figure 5. The transmission coefficients are plotted in a wide band compared to the S$_{11}$ to show the dual-band characteristics of the PA. From Figure 5, it is observed that S$_{21}$ decreases for an increase in temperature.

The main reason for this change is that the mobility of two-dimensional electron gas decreases, and the threshold voltage shifts forward with the rise in temperature [52].

3) MODELING RESULT OF S$_{22}$ UNDER DIFFERENT TEMPERATURE

The modeling results of S$_{22}$ and the measured results are illustrated in Figure 6 for various temperatures. It may be observed from Figure 6 that the change in the profile of S$_{22}$ concerning the temperature change is different throughout the range of frequency. For example, at 1.76 GHz, S$_{22}$ decreases with increasing temperature, while at 2.14 GHz, S$_{22}$ increases. The main reason for this change is that the optimal matching impedance of transistors at different frequencies is different. When the temperature changes, the optimal matching impedance will also change. Suppose
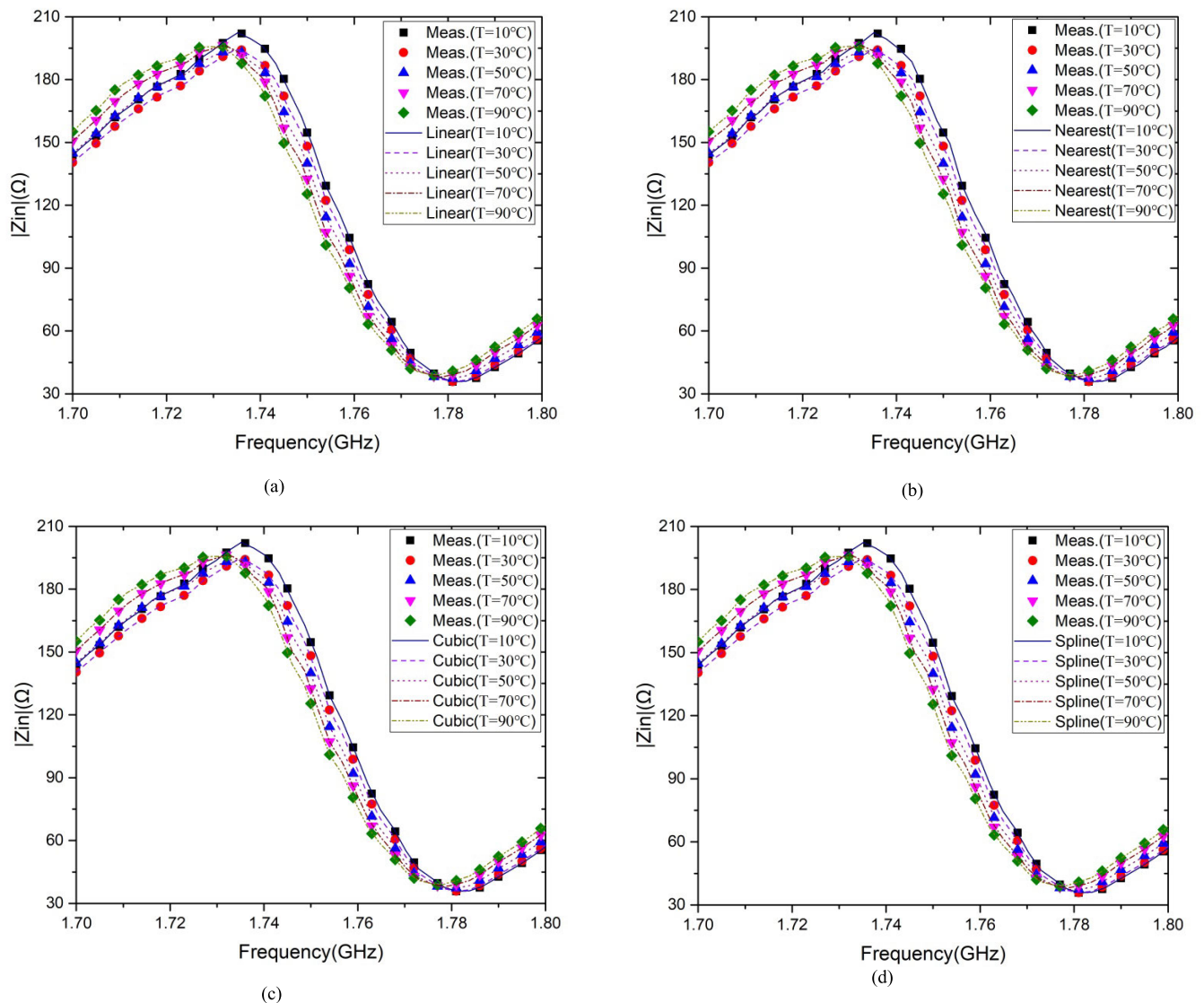
FIGURE 7. The modeling result of input impedance under different temperatures: (a) two-dimensional linear interpolation; (b) two-dimensional nearest interpolation; (c) two-dimensional cubic interpolation;(d) two-dimensional spline interpolation.

the optimal matching impedance at some frequency points is closer to the impedance of the matched circuit that has been manufactured. In that case, it provides a lower reflection loss at that frequency point—otherwise, the value of S_{22} increases.

4) MODELING RESULT OF INPUT IMPEDANCE UNDER DIFFERENT TEMPERATURE

The modeling result of input impedance and the measured values is shown in Figure 7 for various temperatures. As shown in Figure 7, the input impedance varies with temperature at different frequencies. The main reason for this change is that the resistance and capacitance in the transistor change with temperature, which leads to a change of impedance. Since impedance is directly related to capacitance and resistance of a circuit, changes in resistance and capacitance will lead to changes in impedance. Therefore,

it can be observed that the input impedance changes with temperature.

5) MODELING RESULT OF OUTPUT IMPEDANCE UNDER DIFFERENT TEMPERATURE

Similar to the input impedance, the modeling results of output impedance are illustrated in Figure 8 for a range of temperatures. Similar to the input impedance, the output impedance varies with temperature at different frequencies. This variation is also caused by the change in the resistance and capacitance of the transistor with temperature.

6) MODELING RESULT OF STABILITY FACTOR UNDER DIFFERENT TEMPERATURE

The modeling result of the stability factor under different temperatures is illustrated in Figure 9. As shown in Figure 9,
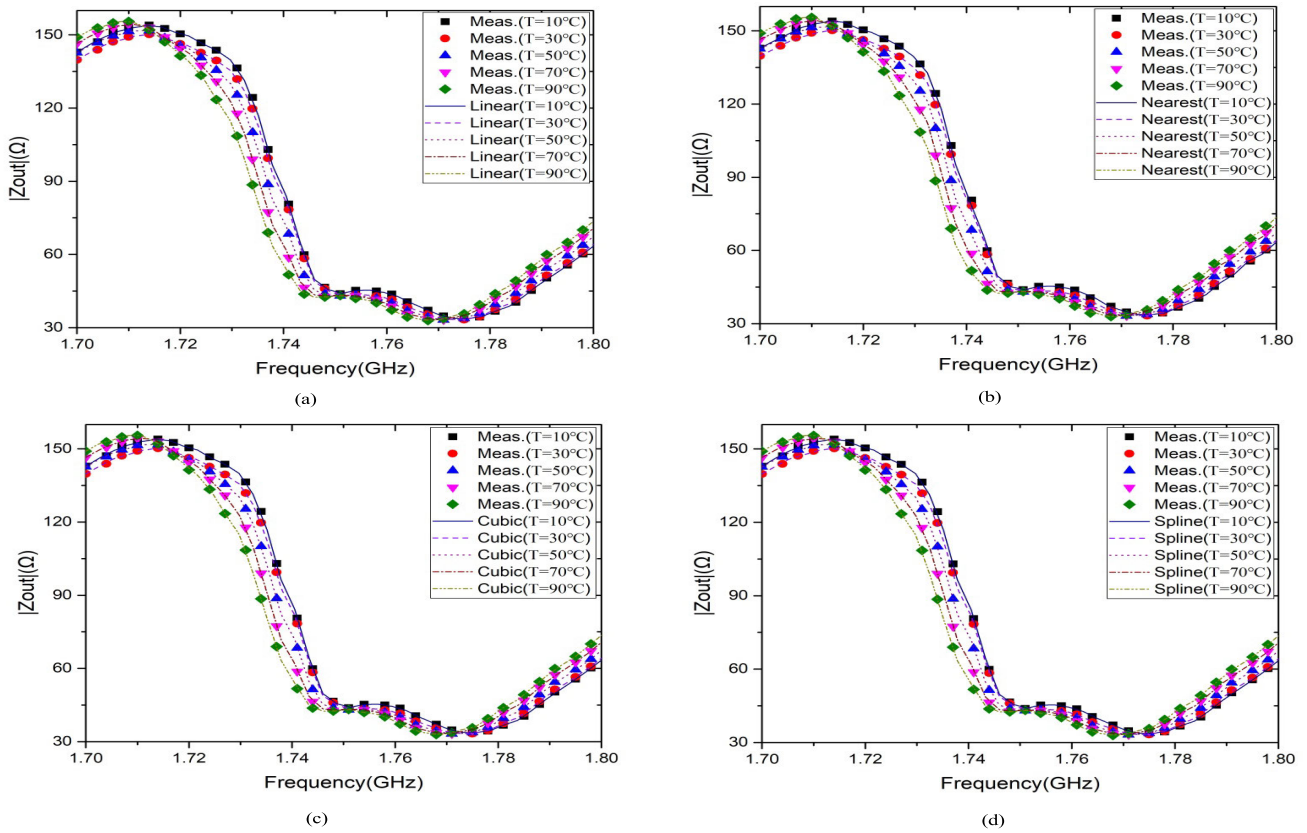
FIGURE 8. The modeling result of output impedance under different temperatures: (a) two-dimensional linear interpolation; (b) two-dimensional nearest interpolation; (c) two-dimensional cubic interpolation;(d) two-dimensional spline interpolation.

The results of the four models are in good agreement with the measurement results.

7) MODELING RESULT OF THE PHASE OF INPUT UNDER DIFFERENT TEMPERATURE

The modeling result from the phase of the input signal under different temperatures is shown in Figure 10. These results show that the nearest model and the measurement results agree only at successive staircase intervals. Due to the inherent quality of the nearest model, continuous agreement with the measured results is not possible. However, the results of the other three models are in decent agreement with the measurement results.

8) MODELING RESULT OF THE PHASE OF OUTPUT UNDER DIFFERENT TEMPERATURE

The modeling result from the phase of the output signal under different temperatures is shown in Figure 11. Like the input signal phase, the only model, i.e., the nearest model results from the output phase, disagrees well with the measurement results. However, the rest of the three models are in good agreement with the measured data.

9) THE MODELING RESULT OF S_{11} UNDER DIFFERENT HUMIDITY

The four kinds of modeling results are estimated using the measured results of PA for various humidity conditions. The measured reflection coefficients (S_{11}) data and the modeled

data are plotted together for each case and given in Figure 12. It is observed that the S_{11} increases with increasing humidity. The main reason for this change can be attributed to the fact that the impedance of the transistor changes with the humidity.

10) THE MODELING RESULT OF S_{21} UNDER DIFFERENT HUMIDITY

The modeling result of the transmission coefficient (S_{21}) data under various humidity conditions is illustrated in Figure 13. From Figure 13, it can be observed that S_{21} decreases with increasing humidity. One of the primary reasons for this change is that the threshold voltage shifts positively [52]. Due to the interchange of the network, the transmission coefficient modeling presented in Figure 13 is valid for S_{12} as well.

11) THE MODELING RESULT OF S_{22} UNDER DIFFERENT HUMIDITY

Since the device is asymmetric, the modeling results extracted from the measured results of S_{22} are also modeled separately and given in Figure 14 for various humidity values. It can be seen from Figure 14 that the change in S_{22} due to humidity is significant in the passband of frequencies. One of the primary reasons for this change is that the humidity changes the resistance and capacitance values in the transistor, which leads to the change of impedance value that brings an inevitable shift in the reflection coefficients.
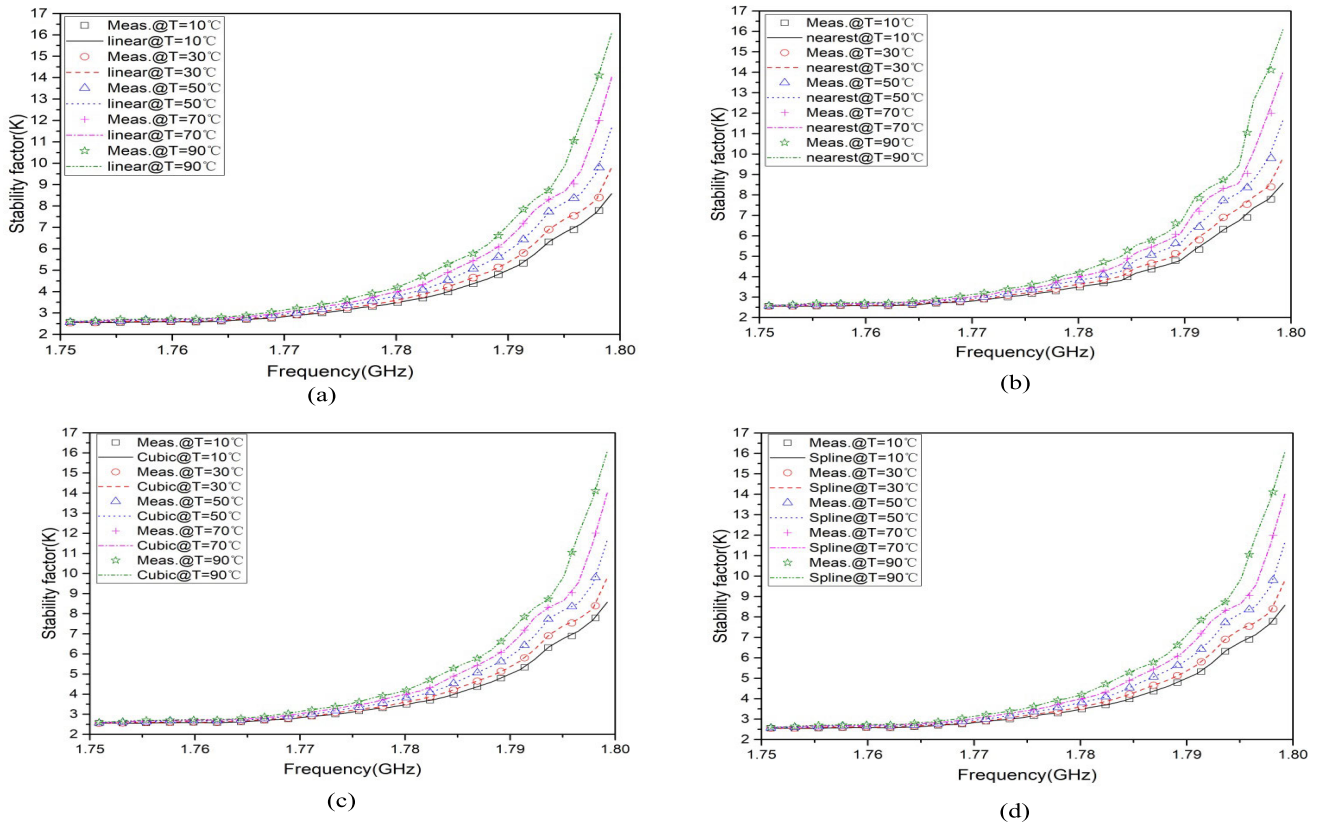
FIGURE 9. The modeling result of stability factor under different temperature: (a) two-dimensional linear interpolation; (b) two-dimensional nearest interpolation; (c) two-dimensional cubic interpolation;(d) two-dimensional spline interpolation.
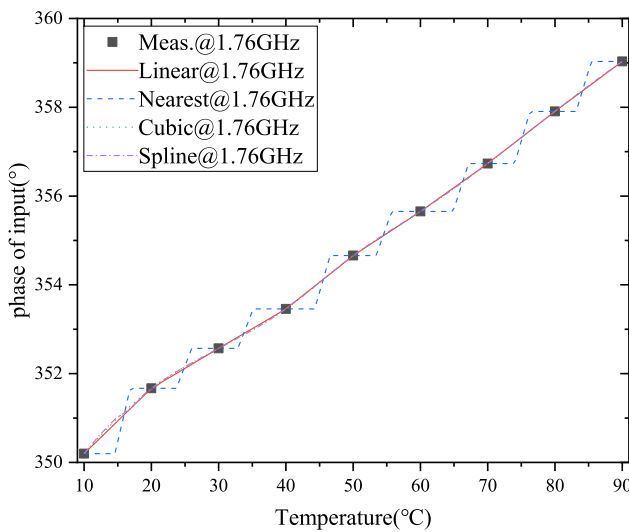

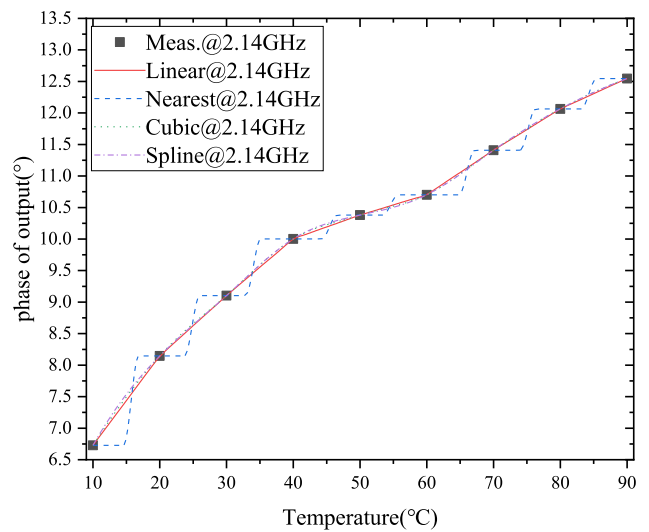**FIGURE 10.** The modeling result of the phase of input under different temperatures.

FIGURE 11. The modeling result of the phase of output under different temperatures.

12) THE MODELING RESULT OF OUTPUT IMPEDANCE UNDER DIFFERENT HUMIDITY

The modeling result of output impedance under different humidity is shown in Figure 15. The results of all four models agree relatively well with the measurements. Still, the model accuracy of the two-dimensional nearest interpolation model

at individual measurement points is not as good as the rest of the three models.

13) THE MODELING RESULT OF THE PHASE OF INPUT/OUTPUT UNDER DIFFERENT HUMIDITY

The modeling result of the input and output signal phase under different humidity conditions are shown
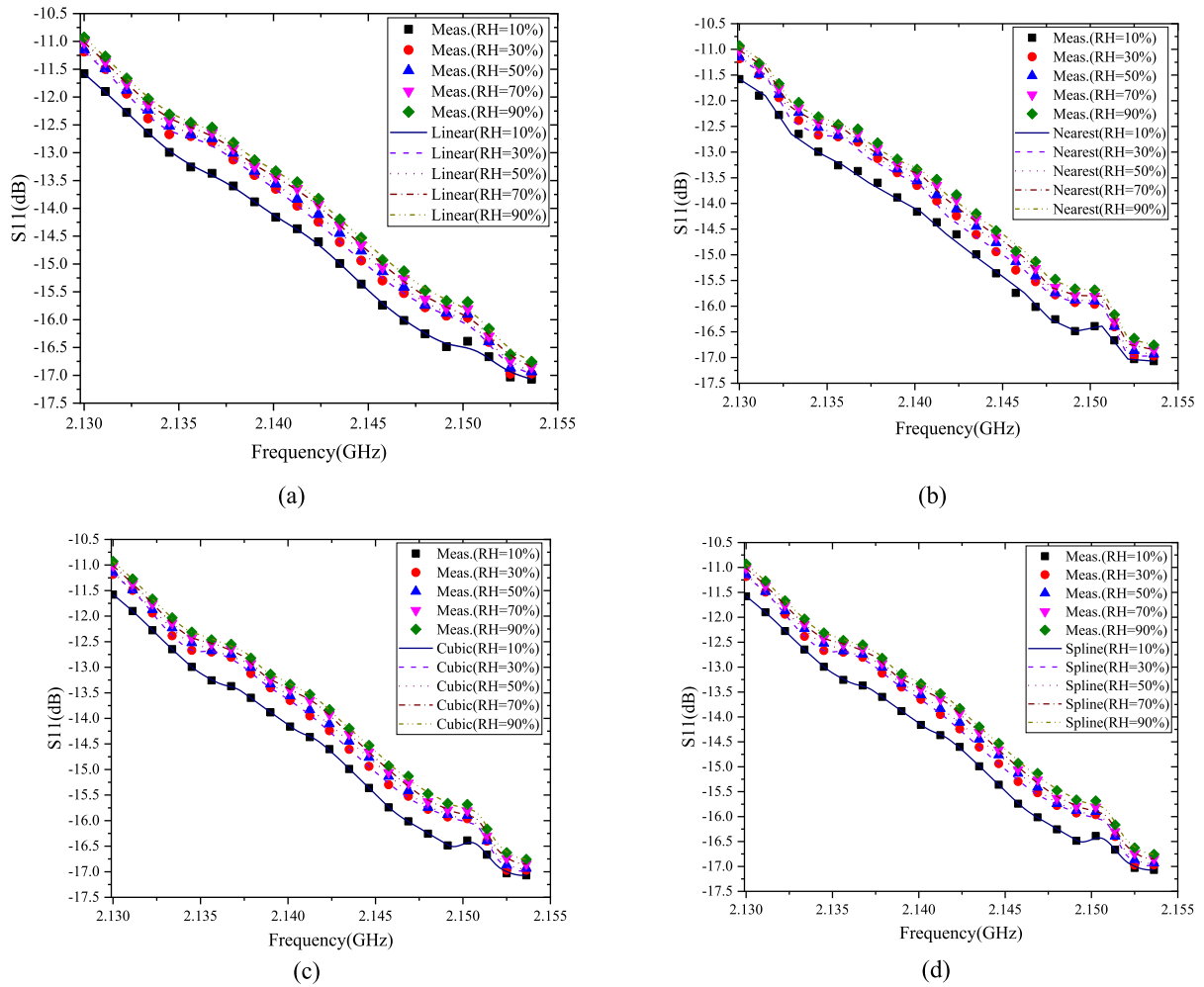
FIGURE 12. The modeling result of S_{11} under different humidity: (a) two-dimensional linear interpolation; (b) two-dimensional nearest interpolation; (c) two-dimensional cubic interpolation; (d) two-dimensional spline interpolation.

in Figures 16 and 17. It is observed that the nearest model and the measurement results are not in excellent agreement. However, the results of the rest of the three models are in good agreement with the measurement results.

## C. MODEL ACCURACY COMPARISON

The testing results of four two-dimensional interpolation models under different temperature and humidity environments are shown in Table 1.

As shown in Table 1, the prediction results of the four different two-dimensional interpolation models are in good agreement with the measurement results. This shows that the two-dimensional interpolation model can be effectively used to predict the temperature and humidity characteristics of the RF power amplifier. Thus, by using a two-dimensional interpolation model to predict the temperature and humidity characteristics of PA, the measurement time and cost can be significantly reduced, and the advanced prediction of PA characteristics under different temperature and humidity conditions can be realized, which is of great significance

for practical application systems, especially for outdoor systems.

As can be seen from Table 1, the method of two-dimensional nearest interpolation has the worst accuracy, but the time of the training model is the shortest. On the other hand, the two-dimensional cubic interpolation and spline interpolation methods have the same accuracy. It may be noted here that the method of two-dimensional cubic interpolation possesses the highest accuracy, while the training time is a trade-off. However, the method of two-dimensional linear interpolation has no significant advantage in terms of either accuracy or time.

Therefore, in selecting a two-dimensional interpolation model to predict the temperature and humidity characteristics of the RF PA, it is necessary to compromise the model training time and model accuracy. To understand the change in the output characteristics of PA subjected to various environmental conditions, *viz.* temperature and humidity, one can use the two-dimensional nearest interpolation model with the shortest model training time. While the precise knowledge
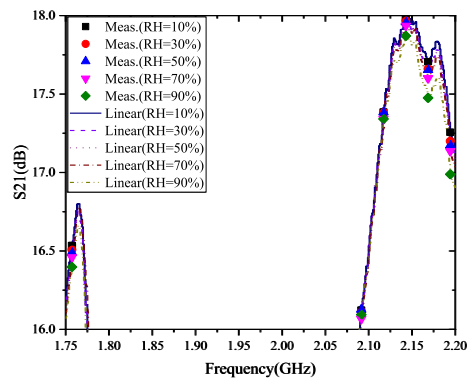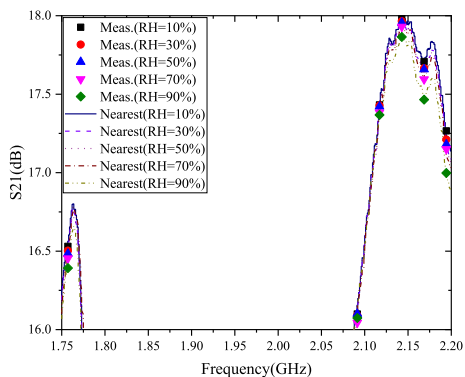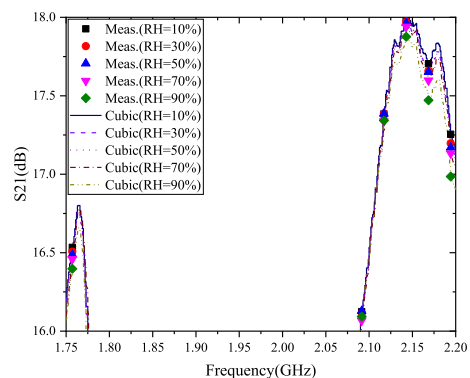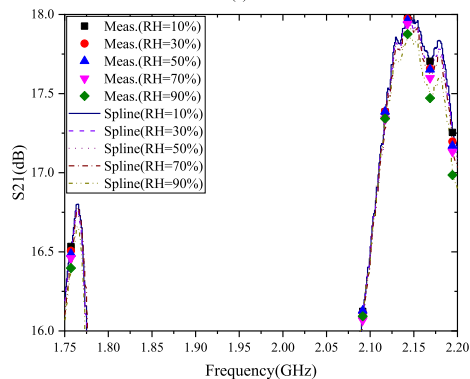
FIGURE 13. The modeling result of S_{21} under different humidity: (a) two-dimensional linear interpolation; (b) two-dimensional nearest interpolation; (c) two-dimensional cubic interpolation; (d) two-dimensional spline interpolation.

FIGURE 14. The modeling result of S_{22} under different humidity: (a) two-dimensional linear interpolation; (b) two-dimensional nearest interpolation; (c) two-dimensional cubic interpolation; (d) two-dimensional spline interpolation.
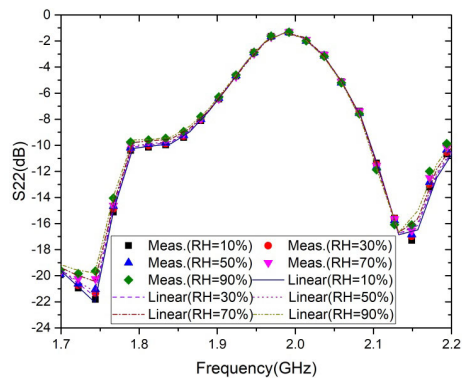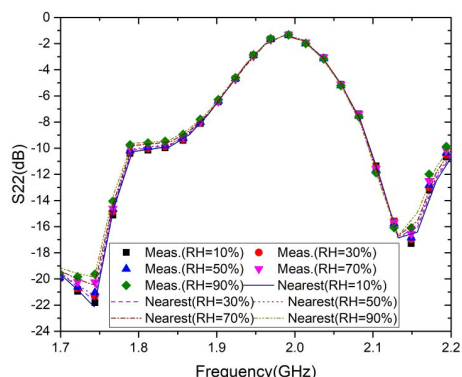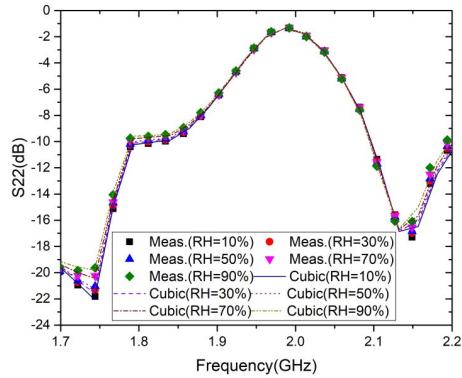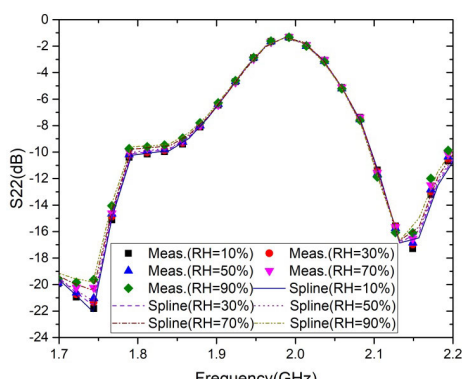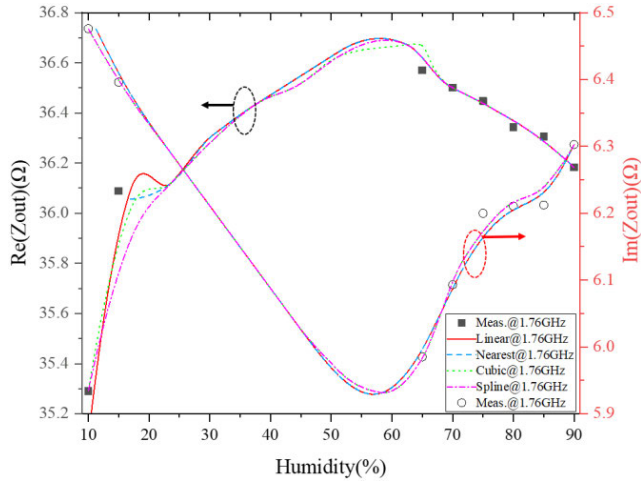
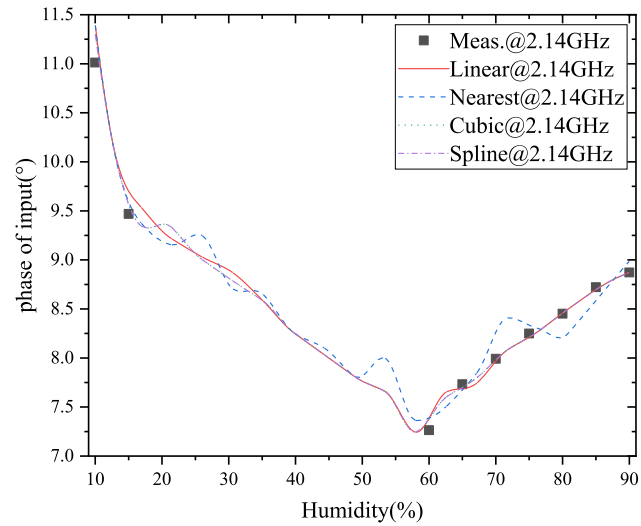**FIGURE 15.** The modeling result of output impedance under different humidity.

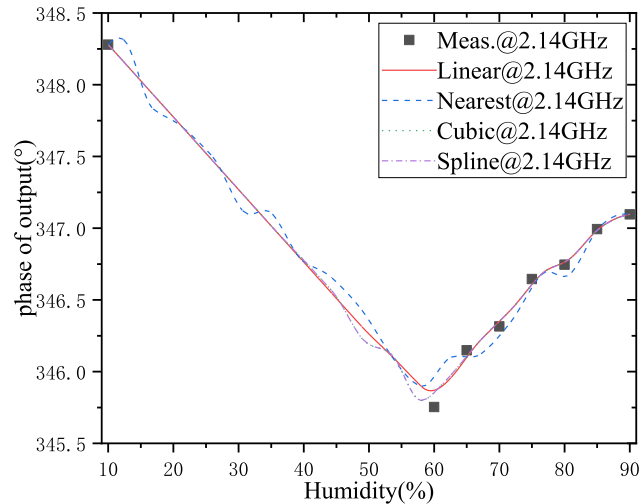**FIGURE 16.** The modeling result of the phase of input under different humidity.

FIGURE 17. The modeling result of the phase of output under different humidity.

TABLE 1. Model Accuracy Comparison Between Four Two-Dimensional Interpolation Under Different Temperature and Humidity Conditions.

Condition	Key Specification of PA	Model Type	Time of Training Model (s)	Test error (RMSE)
Temperature	S11	Linear	0.083	0.0788
		Nearest	0.0771	0.09302
		Cubic	0.166	0.0076
		Spline	0.158	0.0076
	S21	Linear	0.0807	0.0052
		Nearest	0.0758	0.0362
		Cubic	0.1603	0.0016
		Spline	0.1554	0.0016
	S22	Linear	0.0804	0.0245
		Nearest	0.075	0.0422
		Cubic	0.1645	0.0176
		Spline	0.1522	0.0176
	input impedance	Linear	0.0779	0.0248
		Nearest	0.0743	0.0424
		Cubic	0.1605	0.0143
		Spline	0.148	0.0143
	output impedance	Linear	0.0774	0.029
		Nearest	0.0734	0.036
		Cubic	0.1635	0.0288
		Spline	0.1526	0.0288
	Stability factor	Linear	0.0778	0.0093
		Nearest	0.0729	0.088
		Cubic	0.1598	0.0049
		Spline	0.146	0.0049
	Phase of input	Linear	0.0792	0.0120
		Nearest	0.0762	0.0313
		Cubic	0.1545	0.0057
		Spline	0.1494	0.0057
	Phase of output	Linear	0.0841	0.0113
		Nearest	0.0811	0.0420
		Cubic	0.1618	0.0048
		Spline	0.1565	0.0048
Humidity	S11	Linear	0.0804	0.0081
		Nearest	0.0746	0.0115
		Cubic	0.1569	0.0065
		Spline	0.1489	0.0065
	S21	Linear	0.0806	0.0065
		Nearest	0.0741	0.0105
		Cubic	0.1622	0.0022
		Spline	0.1533	0.0022
	S22	Linear	0.0817	0.0517
		Nearest	0.0768	0.0668
		Cubic	0.1613	0.0438
		Spline	0.1564	0.0438
	output impedance	Linear	0.0796	0.0643
		Nearest	0.0746	0.08
		Cubic	0.1588	0.0259
		Spline	0.1517	0.0259
	Phase of input	Linear	0.0796	0.0247
		Nearest	0.0729	0.0334
		Cubic	0.16	0.0205
		Spline	0.1541	0.0205
	Phase of output	Linear	0.0805	0.0378
		Nearest	0.0739	0.0696
		Cubic	0.1574	0.0351
		Spline	0.1465	0.0351

of the output characteristics of a PA operating at a specific temperature and humidity conditions can be estimated using the two-dimensional spline model with the highest model accuracy and shorter model training time. Suppose one wants

to precisely know the performance of a PA at a specific temperature or humidity without spending too much time. In that case, a two-dimensional linear interpolation method can be considered.

IV. CONCLUSION

To obtain the output characteristics of the PA in a wide range of temperature and humidity conditions, a measurement-based modeling method has been proposed in this paper. The proposed method uses four different two-dimensional interpolation models. The results show that the prediction results of these two-dimensional interpolation models are in good agreement with the measurement results. At the same time, the model training time and model accuracy of the four models are compared. The results show that the model accuracy of the two-dimensional nearest interpolation is the worst, but its model training time is the shortest. On the other hand, two-dimensional cubic interpolation and two-dimensional spline interpolation have the same and highest model accuracy, while the model training time of two-dimensional cubic interpolation is the longest. The results of this article guide how to select models for the RF power amplifier or other circuit characteristics prediction.

The modeling method proposed in this paper can predict the performance of the RF power amplifier in the whole temperature and humidity range based on a few key test points, which significantly reduces the measurement time and cost, and can realize the prediction of temperature and humidity characteristics of the RF power amplifier in advance, which is of great significance for practical application systems, especially for outdoor systems. Furthermore, this method is also applicable to predicting and modeling critical specification degradation of other RF/microwave circuits and devices.

REFERENCES

[1] A. Raffo, G. Avolio, V. Vadala, G. Bosi, G. Vannini, and D. Schreurs, "Assessing GaN FET performance degradation in power amplifiers for pulsed radar systems," *IEEE Microw. Wireless Compon. Lett.*, vol. 28, no. 11, pp. 1035–1037, Nov. 2018.

[2] C. Arnaud, D. Basataud, J. Nebus, J. Teyssier, J. Villotte, and D. Floriot, "An active pulsed RF and pulsed DC load-pull system for the characterization of HBT power amplifiers used in coherent radar and communication systems," *IEEE Trans. Microw. Theory Techn.*, vol. 48, no. 12, pp. 2625–2629, Dec. 2000.

[3] B. Chen, L. Lou, K. Tang, Y. Wang, J. Gao, and Y. Zheng, "A 13.5–19 GHz 20.6-dB gain CMOS power amplifier for FMCW radar application," *IEEE Microw. Wireless Compon. Lett.*, vol. 27, no. 4, pp. 377–379, Apr. 2017.

[4] J.-J. Lin, K.-H. To, D. Hammock, B. Knappenberger, M. Majerus, and W. M. Huang, "Power amplifier for 77-GHz automotive radar in 90-nm LP CMOS technology," *IEEE Microw. Wireless Compon. Lett.*, vol. 20, no. 5, pp. 292–294, May 2010.

[5] L. Chen, L. Zhang, and Y. Wang, "A 26.4-dB gain 15.82-dBm 77-GHz CMOS power amplifier with 15.9% PAE using transformer-based quadrature coupler network," *IEEE Microw. Wireless Compon. Lett.*, vol. 30, no. 1, pp. 78–81, Jan. 2020.

[6] H.-Y. Chang, H. Wang, M. Yu, and Y. Shu, "A 77-GHz MMIC power amplifier for automotive radar applications," *IEEE Microw. Wireless Compon. Lett.*, vol. 13, no. 4, pp. 143–145, Apr. 2003.

[7] M. G. Zanchi, P. Stang, A. Kerr, J. M. Pauly, and G. C. Scott, "Frequency-offset Cartesian feedback for MRI power amplifier linearization," *IEEE Trans. Med. Imag.*, vol. 30, no. 2, pp. 512–522, Feb. 2011.

[8] X. Perpina, F. Reverter, J. Leon, E. Barajas, M. Vellvehi, X. Jorda, and J. Altet, "Output power and gain monitoring in RF CMOS class a power amplifiers by thermal imaging," *IEEE Trans. Instrum. Meas.*, vol. 68, no. 8, pp. 2861–2870, Aug. 2019.

[9] J. Park, C. Hu, X. Li, Q. Zhou, and K. K. Shung, "Wideband linear power amplifier for high-frequency ultrasonic coded excitation imaging," *IEEE Trans. Ultrason., Ferroelectr., Freq. Control*, vol. 59, no. 4, pp. 825–832, Apr. 2012.

[10] N. Srirattana, A. Raghavan, D. Heo, P. E. Allen, and J. Laskar, "Analysis and design of a high-efficiency multistage Doherty power amplifier for wireless communications," *IEEE Trans. Microw. Theory Techn.*, vol. 53, no. 3, pp. 852–860, Mar. 2005.

[11] Y. Chung, J. Jeong, Y. Wang, D. Ahn, and T. Itoh, "Power level-dependent dual-operating mode LDMOS power amplifier for CDMA wireless base-station applications," *IEEE Trans. Microw. Theory Techn.*, vol. 53, no. 2, pp. 739–746, Feb. 2005.

[12] M. S. Khan, H. Zhang, X. Wang, R. Ullah, I. Ahmad, and S. Shahzad, "A novel two-stage broadband Doherty power amplifier for wireless applications," *IEEE Microw. Wireless Compon. Lett.*, vol. 28, no. 1, pp. 40–42, Jan. 2018.

[13] C. Liu, H. Xiao, Q. Wu, and F. Li, "Spectrum design of RF power amplifier for wireless communication systems," *IEEE Trans. Consum. Electron.*, vol. 48, no. 1, pp. 72–80, Feb. 2002.

[14] Y. Zhou, P. J. McLane, and C. Loo, "Performance of predistorted APK modulation for one- and two-link nonlinear power amplifier satellite communication channels," *IEEE Trans. Veh. Technol.*, vol. 54, no. 2, pp. 629–638, Mar. 2005.

[15] J. R. Legarra, J. Cusick, R. Begum, P. Kolda, and M. Cascone, "A 500-W coupled-cavity TWT for Ka-band communication," *IEEE Trans. Electron Devices*, vol. 52, no. 5, pp. 665–668, May 2005.

[16] K. Sekine, Y. Dooi, A. Iso, H. Funaki, and I. Takei, "UHF band high-efficiency linear power amplifier for mobile communication satellites," *Electron. Lett.*, vol. 26, no. 7, pp. 441–442, Mar. 1990.

[17] S. R. Boroujeni, A. Basaligheh, S. Ituah, M.-R. Nezhad-Ahmadi, and S. Safavi-Naeini, "A broadband high-efficiency continuous class-AB power amplifier for millimeter-wave 5G and SATCOM phased-array transmitters," *IEEE Trans. Microw. Theory Techn.*, vol. 68, no. 7, pp. 3159–3171, Jul. 2020.

[18] G. Formicone, J. Burger, J. Custer, W. Veitschegger, G. Bosi, A. Raffo, and G. Vannini, "A GaN power amplifier for 100 VDC bus in GPS L-band," in *Proc. IEEE Top. Conf. RF/Microw. Power Modeling Radio Wireless Appl. (PAWR)*, Phoenix, AZ, USA, Jan. 2017, pp. 100–103.

[19] H. Wu, K. S. Yuk, C. Cui, and G. R. Branner, "High power class F GaN HEMT power amplifier in L band for global positioning systems application," in *Proc. IEEE 19th Wireless Microw. Technol. Conf. (WAMICON)*, Sand Key, FL, USA, Apr. 2018, pp. 1–4.

[20] C. Hsieh, J. Roeber, A. Baenisch, A. Hagelauer, T. Ussmueller, and R. Weigel, "A low power CMOS transmitter with class-E power amplifiers for positioning application in multi-band," in *Proc. German Microw. Conf. (GeMiC)*, Bochum, Germany, Mar. 2016, pp. 433–436.

[21] R. Giofrè, P. Colantonio, L. Gonzalez, L. Cabria, and F. De Arriba, "A 300 W complete GaN solid state power amplifier for positioning system satellite payloads," in *IEEE MTT-S Int. Microw. Symp. Dig.*, San Francisco, CA, USA, May 2016, pp. 1–3.

[22] T. Murakami, N. Honma, K. Nishimori, R. Kudo, Y. Takatori, and M. Mizoguchi, "Multi site MIMO channel analysis at 4.85 GHz in outdoor environment," in *Proc. IEEE 20th Int. Symp. Pers., Indoor Mobile Radio Commun.*, Tokyo, Japan, Sep. 2009, pp. 3005–3009.

[23] N. Bel-Haj-Maati, N. Malhouroux, P. Pajusco, and M. Ney, "Mobile measurements at 3.7 GHz using a massive MIMO antenna array in out-door environments," in *Proc. 14th Eur. Conf. Antennas Propag. (EuCAP)*, Copenhagen, Denmark, Mar. 2020, pp. 1–5.

[24] B.-K. Kim, W. L. Stutzman, and D. G. Sweeney, "Indoor and outdoor measurements of space, polarization, and angle diversity for cellular base stations in urban environments," in *Proc. Veh. Technol. Conf. Fall IEEE VTS Fall VTC. 52nd Veh. Technol. Conf.*, Boston, MA, USA, Sep. 2000, pp. 22–29.

[25] Y. C. Lin and J. Zhong, "A review of the influencing factors on anisotropic conductive adhesives joining technology in electrical applications," *J. Mater. Sci.*, vol. 43, no. 9, pp. 3072–3093, May 2008.

[26] Q. Xing. (Mar. 9, 2018). *China Military*. [Online]. Available: http://www.81.cn/jfjbmap/content/2018-03/09/content_201251.htm

[27] H. Lee, J. Tak, and J. Choi, "Wearable antenna integrated into military berets for indoor/outdoor positioning system," *IEEE Antennas Wireless Propag. Lett.*, vol. 16, pp. 1919–1922, 2017.

[28] K. N. Paracha, S. K. A. Rahim, P. J. Soh, M. R. Kamarudin, K.-G. Tan, Y. C. Lo, and M. T. Islam, "A low profile, dual-band, dual polarized antenna for indoor/outdoor wearable application," *IEEE Access*, vol. 7, pp. 33277–33288, 2019.

[29] L. Ahumada, R. Feick, R. A. Valenzuela, and C. Hermosilla, "Measured improvement of indoor coverage for fixed wireless loops with multiple antenna receivers," *IEEE Antennas Wireless Propag. Lett.*, vol. 7, pp. 485–488, 2008.

[30] M. Groth, M. Rzymowski, K. Nyka, and L. Kulas, "ESPAR antenna-based WSN node with DoA estimation capability," *IEEE Access*, vol. 8, pp. 91435–91447, 2020.

[31] S. A. Albahrani, D. Mahajan, S. Kargarrazi, D. Schwantuschke, T. Gneiting, D. G. Senesky, and S. Khandelwal, "Extreme temperature modeling of AlGaN/GaN HEMTs," *IEEE Trans. Electron Devices*, vol. 67, no. 2, pp. 430–437, Feb. 2020.

[32] S. Ghosh, S. A. Ahsan, Y. S. Chauhan, and S. Khandelwal, "Modeling of source/drain access resistances and their temperature dependence in GaN HEMTs," in *Proc. IEEE Int. Conf. Electron Devices Solid-State Circuits (EDSSC)*, Hong Kong, Aug. 2016, pp. 247–250.

[33] M. A. Alim, A. A. Rezazadeh, C. Gaquiere, M. M. Ali, and N. Haris, "0.25 μm AlGaN/GaN HEMT nonlinearity modelling and characterization over a wide temperature range," in *Proc. 10th Eur. Microw. Integr. Circuits Conf. (EuMIC)*, Paris, France, Sep. 2015, pp. 140–143.

[34] S.-H. Zhoul, H.-P. Fu, J.-G. Ma, and Q.-J. Zhang, "A neural network modeling approach to power amplifiers taking into account temperature effects," in *IEEE MTT-S Int. Microw. Symp. Dig.*, Philadelphia, PA, USA, Jun. 2018, pp. 1028–1031.

[35] Q. Lin, Q.-F. Cheng, J.-J. Gu, Y. Zhu, C. Chen, and H.-P. Fu, "Design and temperature reliability testing for a 0.6–2.14 GHz broadband power amplifier," *J. Electron. Test.*, vol. 32, no. 2, pp. 235–240, Apr. 2016.

[36] Q. Lin, H. Fu, Q. Cheng, and Y. Zhu, "Study of the index failure for power amplifier caused by temperature," *Anal. Integr. Circuits Signal Process.*, vol. 89, no. 1, pp. 177–183, Jul. 2016.

[37] Q. Lin, H. Wu, and X. Li, "Study of temperature reliability for a parallel high-efficiency class-E power amplifier," *Circuit World*, vol. 43, no. 3, pp. 111–117, Aug. 2017.

[38] Q. Qi and Z. Chen, "A K-band CMOS amplifier with temperature compensation for gain variation reduction," *IEEE Microw. Wireless Compon. Lett.*, vol. 28, no. 2, pp. 150–152, Feb. 2018.

[39] X. Aragones, E. Barajas, A. Crespo-Yepes, D. Mateo, R. Rodriguez, J. Martin-Martinez, and M. Nafria, "Aging in CMOS RF linear power amplifiers: An experimental study," *IEEE Trans. Microw. Theory Techn.*, vol. 69, no. 2, pp. 1453–1463, Feb. 2021.

[40] T. Hisaka, Y. Aihara, Y. Nogami, H. Sasaki, Y. Uehara, N. Yoshida, and K. Hayashi, "Degradation mechanisms of GaAs PHEMTs in high humidity conditions," in *Proc. JEDEC (Formerly GaAs REL Workshop) ROCS Workshop*, Monterey, CA, USA, 2004, pp. 81–88.

[41] C. Y. Li, T. Yoshida, K. Katayama, M. Motoyoshi, K. Takano, S. Amakawa, and M. Fujishima, "Evaluation of temperature dependence and lifetime of 79 GHz power amplifier," in *Proc. IEEE Int. Meeting Future Electron Devices, Kansai*, Suita, Japan, Jun. 2013, pp. 100–101.

[42] T. Yoshida, K. Takano, C. Li, M. Motoyoshi, K. Katayama, S. Amakawa, and M. Fujishima, "CMOS power amplifier with temperature compensation for 79 GHz radar system," in *Proc. Asia–Pacific Microw. Conf. Proc. (APMC)*, Seoul, South Korea, Nov. 2013, pp. 239–241.

[43] M. Motoyoshi, K. Takano, T. Yoshida, K. Katayama, S. Amakawa, and M. Fujishima, "79 GHz CMOS power amplifier using temperature compensation bias," in *Proc. 9th Eur. Microw. Integr. Circuit Conf.*, Rome, Italy, Oct. 2014, pp. 49–52.

[44] T. Hisaka, H. Sasaki, Y. Nogamni, K. Hosogi, N. Yoshida, A. Villanueva, J. del Alamo, S. Hasegawa, and H. Asahi, "Degradation mechanisms of GaAs PHEMTs under operation in high humidity conditions," in *Proc. ROCS Workshop [Reliability Compound Semiconductors Workshop]*, Monterey, CA, USA, 2008, pp. 109–122.

[45] G. Crupi, A. Raffo, G. Avolio, D. M. M.-P. Schreurs, G. Vannini, and A. Caddemi, "Temperature influence on GaN HEMT equivalent circuit," *IEEE Microw. Wireless Compon. Lett.*, vol. 26, no. 10, pp. 813–815, Oct. 2016.

[46] S. Nuttinck, E. Gebara, J. Laskar, B. Wagner, and M. Harris, "RF performance and thermal analysis of AlGaN/GaN power HEMTs in presence of self-heating effects," in *IEEE MTT-S Int. Microw. Symp. Dig.*, Seattle, WA, USA, Jun. 2002, pp. 921–924.

[47] S. Zhou, "Experimentally investigating the degradations of the GaN PA indexes under different temperature conditions," *Microw. Opt. Technol. Lett.*, vol. 63, no. 3, pp. 758–763, Mar. 2021.

[48] S. Zhou, "Experimental investigation on the performance degradations of the GaN class-F power amplifier under humidity conditions," *Semicond. Sci. Technol.*, vol. 36, no. 3, Feb. 2021, Art. no. 035025.

[49] T. Yoshida, K. Takano, C. Y. Li, K. Katayama, S. Amakawa, and M. Fujishima, "79 GHz CMOS power amplifier considering time-and temperature-degradation model," in *Proc. Asia–Pacific Microw. Conf.*, Sendai, Japan, Nov. 2014, pp. 637–639.

[50] J. Lee and K. Yang, "Temperature-dependent characteristics of InP-RTD-based microwave amplifier IC," *Electron. Lett.*, vol. 53, no. 15, pp. 1058–1060, 2017.

[51] C.-Y. Zhang, Y.-Y. Zhu, Q.-F. Cheng, H.-P. Fu, J.-G. Ma, and Q.-J. Zhang, "Extreme learning machine for the behavioral modeling of RF power amplifiers," in *IEEE MTT-S Int. Microw. Symp. Dig.*, Honolulu, HI, USA, Jun. 2017, pp. 558–561.

[52] S. Zhou, "Experimentally investigating the degradations of small-signal gain for a GaN class-AB dual-band power amplifier under high temperature and humidity conditions," *AIP Adv.*, vol. 10, no. 12, Dec. 2020, Art. no. 125219.

SHAOHUA ZHOU (Student Member, IEEE) received the B.S. degree in microelectronics from Hefei University of Technology, Hefei, China, in 2016. He is currently pursuing the Ph.D. degree in microelectronics and solid-state electronics with Tianjin University, Tianjin, China. His research interests include microwave circuit design and modeling, performance degradations of RF circuits, terahertz detector, and modeling of interconnects.

ABHISHEK KUMAR JHA (Member, IEEE) received the Ph.D. degree in RF and microwaves from the Indian Institute of Technology (IIT), Kanpur, India, in 2017.

He was a Postdoctoral Research Fellow with the Institute of Photonics and Electronics, Prague, Czechia. In 2018, he joined the Microwave and Antenna Engineering Department, Gdansk University of Technology (GUT), Gdansk, Poland. Since 2021, he has been with the Department of Electrical Engineering, IIT, Tirupati, India. He has authored/coauthored more than 50 articles in peer-reviewed international journals and conference proceedings. His current research interests include the numerical analysis and design of novel microwave circuits and waveguide components, the development of RF and microwave sensors for nondestructive testing, and measurements of intrinsic and physical properties.

Dr. Jha received several awards, including the IDUB Premium Award 2020 by the Rector of GUT, the highly prestigious Microwave Graduate Fellowship Award, USA, in 2015, the Second and Third Prizes in the IEEE SIGHT DESIGN contest organized by the IEEE MTT and AP Societies 2015, respectively, the two successive University Gold Medals for being first in the first class of B.E. and M.Tech. degrees, in 2009 and 2011, respectively, and the Gandhian Young Technological Innovation Award, in 2016. He garnered research funding under the technological edge category. He founded and chaired the IEEE MTT-S SBC, Kanpur, in 2014. He served as the Chair for the oral session in the IEEE CAMA 2014, France. He is currently serving as the Associate Editor for IEEE ACCESS and IEEE SENSORS and a Potential Reviewer of premier journals, such as the IEEE TRANSACTION ON INDUSTRIAL ELECTRONICS, the IEEE TRANSACTION ON MICROWAVE THEORY AND TECHNIQUES, and the IEEE SENSOR JOURNAL.

● ● ●